J. Mol. Biol. (1997) **272**, 64–81

JMB

The NMR Solution Conformation of Unligated Human Cyclophilin A

Marcel Ottiger, Oliver Zerbe, Peter Güntert and Kurt Wüthrich*

Institut für Molekularbiologie und Biophysik, Eidgenössische Technische Hochschule Hönggerberg, CH-8093, Zürich Switzerland

The nuclear magnetic resonance (NMR) solution structure of free, unligated cyclophilin A (CypA), which is an 18 kDa protein from human T-lymphocytes that was expressed in *Escherichia coli* for the present study, was determined using multidimensional heteronuclear NMR techniques. Sequence-specific resonance assignments for 99.5% of all backbone amide protons and non-labile hydrogen atoms provided the basis for collection of an input of 4101 nuclear Overhauser enhancement (NOE) upper distance constraints and 371 dihedral angle constraints for distance geometry calculations and energy minimization with the programs DIANA and OPAL. The average RMSD values of the 20 best energy-refined NMR conformers relative to the mean coordinates are 0.49 Å for the backbone atoms and 0.88 Å for all heavy atoms of residues 2 to 165. The molecular architecture includes an eight-stranded antiparallel β-barrel that is closed by two amphipathic α-helices. Detailed comparisons with the crystal structure of free CypA revealed subtle but significant conformational differences that can in most cases be related to lattice contacts in the crystal structure. ^{15}N spin relaxation times and NMR lineshape analyses for CypA in the free form and complexed with cyclosporin A (CsA) revealed transitions of polypeptide loops surrounding the ligand-binding site from locally flexible conformations in the free protein, some of which include well-defined conformational equilibria, to well-defined spatial arrangements in the CypA-CsA complex. Compared to the crystal structure of free CypA, where the ligand-binding area is extensively involved in lattice contacts, the NMR structure presents a highly relevant reference for studies of changes in structure and internal mobility of the binding pocket upon ligand binding, and possible consequences of this conformational variability for calcineurin recognition by the CypA-CsA complex.

Keywords: cyclophilin A; cyclosporin A; immunophilins; NMR structure; protein dynamics

**Corresponding author*

Introduction

The protein cyclophilin A (CypA) from human T lymphocytes consists of 165 amino acid residues and possesses peptidyl-prolyl *cis-trans* isomerase activity (Handschumacher *et al.*, 1984; Fischer *et al.*, 1989). CypA has attracted keen interest in biomedical research, since it functions as an intracellular re-

Present addresses: M. Ottiger, Laboratory of Chemical Physics, National Institute of Diabetes and Digestive and Kidney Diseases, National Institutes of Health, Bethesda, MD 20892-0510, USA; O. Zerbe, Departement für Pharmazie, ETH, CH-8057 Zürich, Switzerland.

Abbreviations used: Cyp, cyclophilin; CypA, cyclophilin A; CsA, cyclosporin A; CaN, calcineurin; NMR, nuclear magnetic resonance; NOE, nuclear Overhauser effect; 2D, 3D, 2-,3-dimensional; NOESY, nuclear Overhauser enhancement spectroscopy; COSY, correlation spectroscopy; TOCSY, total correlation spectroscopy; *ct*, constant-time; ppm, parts per million; $^3J_{HN\alpha}$, vicinal spin-spin coupling constant between the backbone amide proton and the α proton; $^3J_{N\beta}$, vicinal spin-spin coupling constant between the backbone amide nitrogen and one of the β protons; $^3J_{\alpha\beta}$, vicinal spin-spin coupling constant between the α proton and one of the β protons; RMSD, root-mean-square deviation; T_1, longitudinal relaxation time; T_2, transverse relaxation time; $T_{1\rho}$, relaxation time in the rotating frame; REDAC, use of redundant dihedral angle constraints.

0022–2836/97/360064–18 $25.00/0/mb971220

ceptor of the immunosuppressive cyclic undecapeptide cyclosporin A (CsA), which acts as an inhibitor of specific signal transduction pathways leading to T lymphocyte activation (Borel, 1986; Schreiber, 1991). Because of its high affinity for this drug, CypA has an important role in the prevention of organ transplant rejection (Borel, 1989). Renewed interest in research about cyclophilin has recently been sparked by the findings that CypA binds to the HIV-1 Gag protein (Luban *et al*., 1993), and that it is specifically incorporated in HIV-1 virions and required for their infectious activity (Franke *et al*., 1994; Thali *et al*., 1994).

Interest in the molecular basis of immunosuppressive action spurred vigorous research on the CypA/CsA system, including three-dimensional structure determinations by nuclear magnetic resonance (NMR) spectroscopy and X-ray crystallography (for a review, see Braun *et al*., 1995). Structural studies of the CypA/CsA system yielded a first important result with the NMR determination of the conformation of CypA-bound CsA (Fesik *et al*., 1991; Weber *et al*., 1991; Wüthrich *et al*., 1991a), which was found to be very different from the structure of free CsA in crystals or in non-polar solvents (Loosli *et al*., 1985). Subsequently, the secondary structure of CypA in solution was determined (Wüthrich *et al*., 1991b), which was then used to support the tracing of a low-resolution electron density map to yield the crystal structure of CypA complexed with a linear tetrapeptide substrate (Kallen *et al*., 1991). On the basis of the crystal structure, the NMR structure of CypA-bound CsA and measurements of intermolecular nuclear Overhauser enhancement (NOE) distance constraints identifying CypA-CsA contacts, a molecular model of the CypA-CsA complex was generated (Spitzfaden *et al*., 1992). Subsequently, a crystal structure of free CypA and more than ten structure determinations of ligated cyclophilins in crystals and in solution have been reported (see Discussion and Table 4 below). We now add the NMR solution structure of free recombinant CypA expressed in *Escherichia coli*, and report comparative studies of internal mobility of CypA in the free form and in the CypA-CsA complex through measurements of ^{15}N spin relaxation times. These data are analyzed with regard to mechanistic aspects of ligand binding by CypA and recognition of the CypA-CsA complex by calcineurin (CaN).

Results

Assignments of the polypeptide backbone and aliphatic side-chain resonances

Complete sequence-specific NMR assignments for free CypA (Table 1) were obtained based nearly entirely on scalar coupling connectivities. Assignments of backbone resonances were established using 3D CBCA(CO)NH (Grzesiek & Bax, 1992) and *ct*-HNCA (Madsen & Sørensen, 1992) spectra. The backbone assignments are in good agreement with those obtained previously (Spitzfaden *et al*., 1992), using amino acid identification with residue-specific ^{15}N labeling (Wüthrich *et al*., 1991a) and 3D ^{15}N-resolved [^1H, ^1H]-NOESY and 3D ^{15}N-resolved [^1H, ^1H]-TOCSY (Fesik & Zuiderweg, 1988) for the identification of sequential NOE connectivities (Wüthrich, 1986). Some small shift differences between the two data sets are due to changes in buffer conditions. The ^{13}C chemical shifts of the $C^{\alpha}H$-$C^{\beta}H_n$ fragments provided the starting point for the complete ^1H and ^{13}C assignments of all CH_n moieties in non-aromatic side-chains and the ^1H assignments in the $C^{\beta}H_2$ fragments of aromatic side-chains, using 3D HCCH-TOCSY (Bax *et al*., 1990), 3D CCH-TOCSY (Fogh *et al*., 1995) and 3D HCCH-COSY (Kay *et al*., 1990; Ikura *et al*., 1991). $H^{\gamma 3}$ of Arg19 and Gln111, and the $C^{\gamma}H_2$ group of Arg37 could be assigned only in the 3D ^{13}C-resolved NOESY spectrum. The $C^{\varepsilon}H_3$ assignments for the Met residues were made using a modified HMBC experiment (Bax *et al*., 1994) which, in con-

Table 1. Survey of the results achieved for the sequence-specific resonance assignment and the collection of the input for the structure calculation of CypA

Parameter	Extent[a]	Comments
Squence-specific assignments (%)		
Backbone NH	99.4	Missing: NH of Val2
Aliphatic CH_n	100.0	
Aromatic CH	97.9	Missing: H^{ζ} of Phe36 and Phe60
Labile side-chain protons[b]	71.7	32 NH, 10 OH and 1 SH assigned
Stereospecific (individual) assignments	73	46 CH_2, 16 $C(CH_3)_2$, (11 NH_2)
Unambiguously assigned NOE cross-peaks	7160	
Meaningful NOE upper distance limits[c]	4101	
Coupling constants measured	217	119 $^3J_{HN\alpha}$, 98 $^3J_{N\beta}$
Dihedral angle constraints[d]	371	135 ϕ, 135 ψ, 101 χ^1

[a] The extent is given either as percentage of the total number in CypA, or as an absolute number.
[b] Here, 100% corresponds to all labile side-chain protons of Asn, Cys, Gln, His, Ser, Thr, Trp and Tyr, and H^{ε} of Arg.
[c] After removal of intraresidual NOEs and other NOEs that do not constrain the conformation, as identified by the initial processing with the program DIANA (Güntert *et al*., 1991), and pseudo-atom replacement of the non-degenerate, symmetry-related ring protons of Phe112 and Phe129, and the $N^{\eta}H_2$ groups of Arg19 (Wüthrich *et al*., 1983).
[d] Dihedral angle constraints from the measured coupling constants and the intraresidual and sequential NOEs, using the program HABAS (Güntert *et al*., 1989).

trast to the use in the original paper, was performed in two dimensions.

Among the labile side-chain protons, the SH proton of Cys62 was assigned at 1.60 ppm in TOCSY and NOESY spectra. To our knowledge this is the first time that the chemical shift of a Cys SH proton has been reported for a protein. The amide groups of all Asn and Gln, $N^{\varepsilon}H$ of all Arg, $(N^{\eta}H_2)_2$ of Arg19, $N^{\varepsilon 1}H$ of Trp121 and His92, and the hydroxyl protons of the seryl residues 32, 41, 73, 107, 119 and 152, and the threonyl residues 40, 51, 77 and 110 were assigned by intraresidual NOEs (Wüthrich, 1986). Eight of these assignments were verified in a 2D [^{1}H, H^1]-clean-TOCSY experiment.

Stereospecific assignments for the isopropyl methyl groups of all Val and Leu were obtained by biosynthetically directed fractional ^{13}C labeling (Senn *et al.*, 1989; Neri *et al.*, 1989).

For the residues 2, 4, 24 to 27 and 163 to 165, which are all located spatially close to the N terminus, additional weak signals were identified due to the presence of residual amounts of des-Met CypA which could not be removed during the protein purification. Except for Leu2, for which a complete second spin system was assigned, and Pro4, only the backbone ^{15}N-^{1}H groups of the aforementioned residues gave rise to resolved pairs of peaks. Such extra peaks were present also in the spectra reported in previous NMR studies of the Cyp-CsA complex (Thériault *et al.*, 1993; Spitzfaden *et al.*, 1994) but were not discussed there.

Assignment of the aromatic spin systems

CypA contains a total of 22 aromatic residues, i.e. 15 phenylalanine, two tyrosine, one tryptophan and four histidine residues. The aromatic spin systems were assigned in a 3D ^{1}H-TOCSY-relayed *ct*-[^{13}C, ^{1}H]-HMQC spectrum (Zerbe *et al.*, 1996), and the sequence-specific assignments were obtained *via* scalar connectivities to the previously assigned $C^{\beta}H_2$ groups by $(H^{\beta})C^{\beta}(C^{\gamma}C^{\delta})H^{\delta}$ and $H^{\beta}(C^{\beta}C^{\gamma}C^{\delta})H^{\delta}$ experiments (Yamazaki *et al.*, 1993). The sequence-specific assignments were independently supported by intraresidual NOEs between aromatic and aliphatic protons (Wüthrich, 1986). For the three phenylalanine residues 36, 112 and 129, and for Tyr48, which belong to a group of seven aromatic core residues that point into the interior of the β-barrel and are all involved in direct spatial contact with at least one other ring (Figure 1(b)), the assignment was more involved. Eventually, combined analysis of the following experiments, in conjunction with intramolecular distance information from initial structure calculations, resulted in sequence-specific ^{1}H assignments for these four aromatic spin systems (Figure 2): 2D [^{1}H, ^{1}H]-clean-TOCSY spectra with mixing times of 20 and 40 ms (Braunschweiler & Ernst, 1983; Griesinger *et al.*, 1988); [^{1}H, ^{1}H]-NOESY spectra (Anil-Kumar *et al.*, 1980) with mixing times of 60 and 120 ms recorded in H_2O and ^2H_2O solutions with and without ^{15}N half-filters

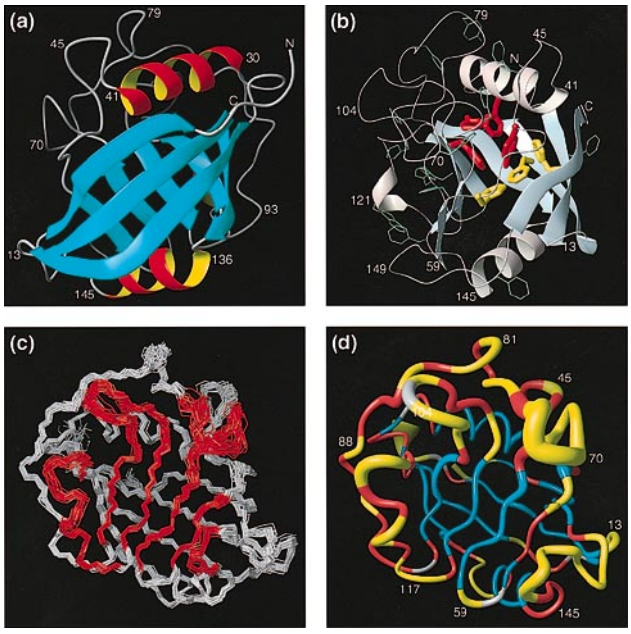

Figure 1. (a) Ribbon drawing of the structure of CypA. The β-strands and helices are drawn as cyan arrows and red-yellow ribbons, respectively, and the intervening turns and loops as gray tubes. The N and C termini and some sequence locations are indicated. (b) Ribbon drawing of CypA with the aromatic core residues Phe112, Phe129, and Phe36 and Tyr48 (red, from left to right) and Phe53, Phe22 and Phe8 (yellow, from left to right). All other aromatic side-chains are drawn as thin green lines. See the text for further details. The orientation of the molecule derives from that in (a) by a counter-clockwise rotation of about 90° around the vertical axis. (c) Polypeptide backbone of the 20 energy-minimized DIANA conformers used to represent the NMR solution structure after superposition for minimal RMSD of the backbone atoms N, C^{α} and C′ of residues 2 to 165. The orientation of the molecule derives from (a) by a 180° rotation about the vertical axis and affords a view of the CsA-binding site, with the polypeptide segments affected by ligand binding shown in red. (d) Backbone of the mean NMR solution structure. A spline function was drawn through the C^{α} positions, and the radius of the cylindrical rod corresponds to the mean of the global displacements, D^{bb}_{glob}. The coloring represents backbone amide proton exchange rates: blue, $k_{HD} \leqslant 10^{-3}$ min^{-1} (very slow exchange; for these positions complete exchange could not be achieved without irreversible denaturation of CypA); red, $< 10^{-3}$ min^{-1} $k_{HD} \leqslant 10^{-1}$ min^{-1}; yellow, $k_{HD} > 10^{-1}$ min^{-1} (rapid exchange; rate outside the range accessible for quantitative measurements with the method used); gray, prolyl residues. These and all other color Figures were generated with the program MOLMOL (Koradi *et al.*, 1996).

(Otting & Wüthrich, 1990); 3D ^{15}N and ^{13}C-resolved [^{1}H, ^{1}H]-NOESY. The chemical shifts of the symmetry-related pairs of ring protons of Phe112 and Phe129 are not degenerate, and the chemical shift differences, Δδ, are all bigger than 0.9 ppm. Therefore, the ring-flip rates must be smaller than the coalescence frequency, which is 1200 s^{-1} at 600 MHz. The observed signals were very broad and

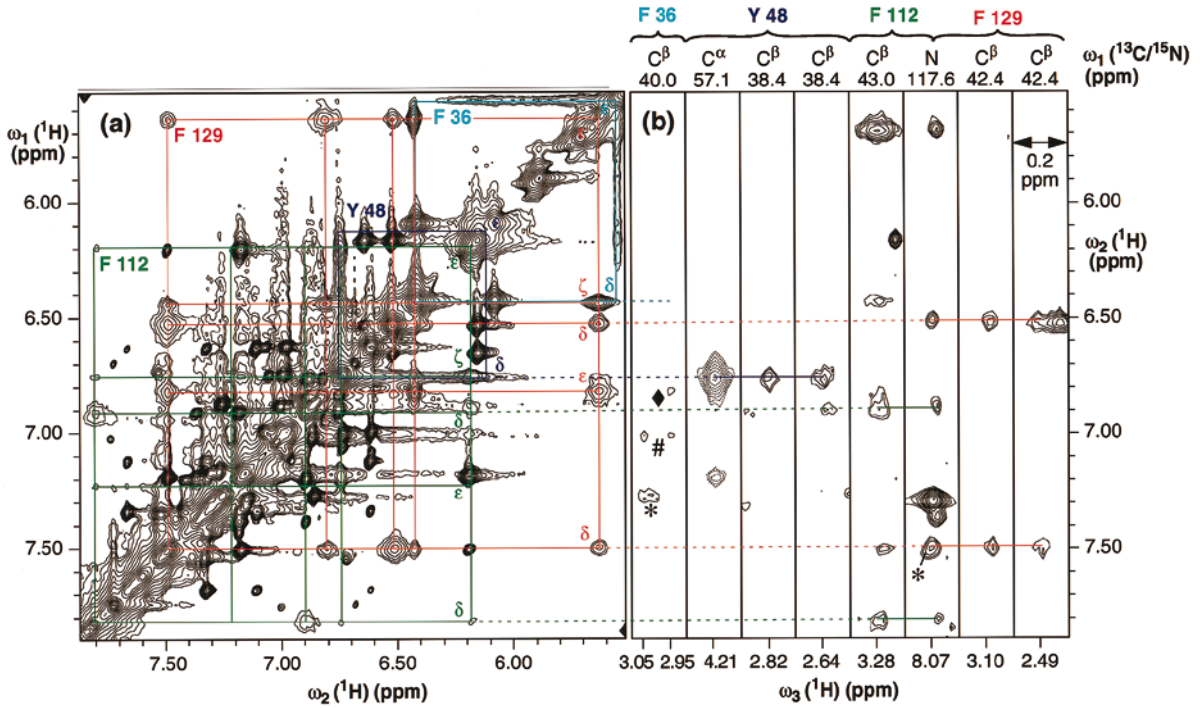

Figure 2. Assignment of the aromatic spin systems of Phe36, Phe112, Phe129 and Tyr48. (a) Contour plot of a spectral region of a 2D [^{1}H, ^{1}H]-TOCSY spectrum recorded with $\tau_m = 20$ ms, which contains all the aromatic spin systems of CypA. The connectivities in the spin systems of Phe36, Phe112, Phe129 and Tyr48 are indicated with colored lines. (b) [$\omega_2(^1H)$,$\omega_3(^1H)$] strips from 3D ^{13}C and ^{15}N-resolved [^{1}H, ^{1}H] NOESY spectra recorded with $\tau_m = 60$ ms. Intraresidual NOEs to the aromatic H$^\delta$ protons are connected with colored lines. The symbols # and ◆ indicate NOEs to HN of Phe36 and H$^\varepsilon$ of Phe129, respectively, which appear to be of low intensity because of exchange broadening although they actually correspond to short distances of about 2.5 Å. The asterisks (*) indicate residual peak intensities belonging to peaks centered in different planes. Aliased signals are drawn with dotted contours. The spectra were recorded with 2 mM solutions of ^{15}N-labeled CypA in 90% H_2O/10% ^2H_2O (2D TOCSY and 3D ^{15}N-resolved NOESY) or ^{13}C-labeled CypA in ^2H_2O (3D ^{13}C-resolved NOESY), pH/pD 6.5, at 26°C.

hence too weak for a quantitative line shape analysis (Figure (2a)). We estimate that the ring flip frequency is about 100 s^{-1}. For Trp121, the protons of the six-membered ring of the indole moiety were connected with the C$^{\delta1}$H signal by 2D *ct*-HCCH-TOCSY (Ikura *et al.*, 1991), and this assignment was verified by intraresidual NOEs. The C$^{\varepsilon1}$H groups of the four histidine residues were assigned by NOEs. Overall, the assignments for the aromatic protons are complete with the sole exceptions of H$^\zeta$ of Phe36 (see below) and Phe60 (which is probably degenerate with the H$^\varepsilon$ protons).

Collection of conformational constraints

A total of 7160 NOE cross-peaks were assigned in 3D ^{15}N-resolved [^{1}H, ^{1}H]-NOESY, 3D ^{13}C-resolved [^{1}H, ^{1}H]-NOESY and 2D [^{1}H, ^{1}H]-NOESY, all with a mixing time of 60 ms. In addition, 119 $^3J_{HN\alpha}$ coupling constants were extracted by inverse Fourier transformation of in-phase multiplets from a 2D [^{15}H, ^{1}H]-HSQC spectrum (Szyperski *et al.*, 1992), and 98 $^3J_{N\beta}$ coupling constants were estimated from 3D *ct*-HNHB (Archer *et al.*, 1991; Chary *et al.*, 1991). Data analysis with the programs HABAS and GLOMSA resulted in stereospecific assignments for 46 CH_2 groups and individual assignments for 11 of the 12 NH_2 groups of Asn and Gln (Table 1). After removal of the distance constraints relating to des-Met CypA, pseudo-atom replacement of the non-degenerate symmetry-related ring protons of Phe112 and 129 and the N$^\eta$H$_2$-groups of Arg19, and an initial screening of the experimental data set with the programs HABAS and DIANA, which removed irrelevant constraints and processed groups of diastereotopic protons for which no stereospecific assignments had been obtained, a final data set of 4101 NOE upper distance limits (662 intraresidual, 948 sequential, 700 medium-range and 1791 long-range) and 371 dihedral angle constraints (135 for ϕ, 135 for ψ and 101 for χ^1) was obtained (Table 1). This corresponds to an average of more than 27 constraints per residue. In general, residues located in regular secondary structures are involved in about 50 up to a maximum of 104 NOE distance constraints, whereas residues in loops are usually involved in less than 30 NOE distance constraints (Figure 3(a)).

The NMR solution structure of CypA

The tertiary fold of free CypA in solution contains the topology of regular secondary structures that was first identified by Wüthrich *et al.* (1991a) using an empirical approach of pattern-recognition

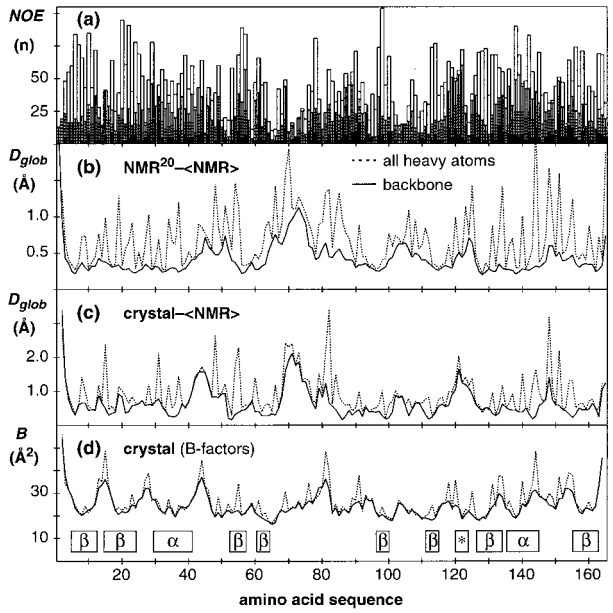

Figure 3. Plots of the number of NOEs, global displacements (D_{glob}) and crystallographic *B*-factors *versus* the amino acid sequence of CypA. (a) Numbers of NOE distance constraints per residue used in the calculation of the CypA structure. Filled, crosshatched, vertically hatched and open bars represent, respectively, intraresidual, sequential, medium-range and long-range NOEs. (b) Mean of the pairwise global displacements per residue of the backbone heavy atoms (continuous line) and all heavy atoms (broken line) of the 20 energy-minimized DIANA conformers (**NMR**^{20}) relative to the mean NMR structure (⟨**NMR**⟩) calculated after superposition of the backbone heavy atoms N, C^{α} and C′ of residues 2 to 165 for minimal RMSD. (c) Global displacements per residue of the backbone heavy atoms (continuous line) and all heavy atoms (broken line) between the crystal structure of free CypA (Ke, 1992) and the mean NMR structure calculated after superposition of the backbone heavy atoms N, C^{α} and C′ of residues 2 to 165 for minimal RMSD. (d) Average temperature factors (*B*) per residue for the backbone heavy atoms (continuous line) and all heavy atoms (broken line) in the crystal structure (Ke, 1992). The locations of the regular secondary structure elements are given at the bottom of the Figure, where α, * and β indicate α-helix, 3_{10}-helix and β-strand, respectively.

in the NMR data (Wüthrich *et al.*, 1984) and has subsequently been observed in all the structure determinations listed in Table 4 (see below). An eight-stranded antiparallel β-barrel encompassing residues 5 to 12, 15 to 24, 53 to 57, 61 to 64, 91 to 100, 112 to 115, 127 to 134 and 156 to 163 is closed by two amphipathic α-helices (residues 30 to 41 and 136 to 145), and a short 3_{10}-helix (residues 120 to 122: Figure 1(a)). In the connections between the regular secondary structure elements, several well-defined β-turns (residues 12 to 15, 42 to 45, 48 to 51, 57 to 60, 77 to 80 and 147 to 150) and β-bulges (residues 17-18/10, 54-55/63, 60-61/57, 129-130/98, 133-134/21 and 159-160/9) could be identified. A survey of the complete structure is given in Figure 4.

In the results of the structure calculation (Table 2) the small size and small number of residual constraint violations show that the input data represents a self-consistent set, and that the constraints are well satisfied in the calculated conformers. The global RMSD values calculated for different atom selections reflect the intrinsically high precision of the structure determination, but locally there are pronounced variations in the precision along the polypeptide chain: secondary structures are usually very well defined, whereas longer loops and the chain termini, especially the N terminus and the segment of residues 65 to 76, show increased structural disorder (Figures 1(c), 3(b) and 4). Among the non-Gly residues, 85% of all side-chains have a global heavy-atoms displacement, D^{sc}_{glob}, of less than 1.0 Å, and 50% of all side-chains have D^{sc}_{glob} values below 0.5 Å (Table 2). All side-chains with D^{sc}_{glob} values higher than 1.0 Å are located on the protein surface, with the sole exception of Tyr48, for which the aromatic ring protons were involved in only a small number of very broad NOE signals (see also Assignment of the aromatic side-chains, above).

Outstandingly large conformation-dependent ^{1}H NMR shifts in amino acid side-chains

In line with the large number of aromatic residues in CypA (see above), the ^{1}H NMR spectrum contains numerous signals with large ring current shifts. Of a total of 27 side-chain resonances with conformation-dependent secondary shifts larger than 1.0 ppm (Table 3), 24 can be qualitatively explained by simple ring current calculations using the final NMR structure (Perkins & Wüthrich, 1979), whereas the remaining three large shifts are dominated by hydrogen bonds or salt-bridge formation. The large ranges of ring current shifts calculated from the individual 20 refined DIANA conformers, which include the experimental value in all but four cases (Table 3), illustrate the extreme sensitivity of ring current shifts to small local variations of the three-dimensional structure (Wüthrich, 1986). As an example, in the mean NMR structure the so far unassigned H^{ζ} of Phe36 is located exactly over the aromatic rings of Tyr48 and Phe112 (Figure 1(b)), with distances of about 3.0 Å to the two ring centers. The calculation of ring current effects (Perkins & Wüthrich, 1979) showed that the contributions in the 20 individual NMR conformers range from −4.18 to +0.14 ppm. Intramolecular motions of the aromatic rings on a millisecond time-scale (see above) would thus cause line broadening by averaging the chemical shift, which might explain why this proton could not be detected.

Discussion

The ligand-binding area of CypA has been characterized at variable degrees of precision in the different structure determinations listed in Table 4.

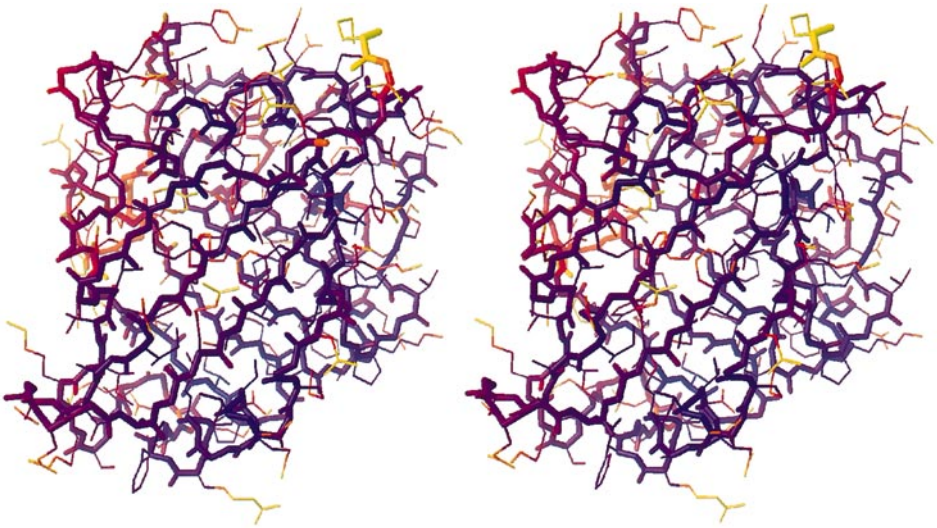

Figure 4. Stereo view of the all-heavy-atom representation of the energy-minimized DIANA conformer with the lowest RMSD value to the mean NMR structure of CypA. The backbone is drawn as a thick line, and the gradual coloring represents the mean of the global displacements of all 20 DIANA conformers (Figure 3(b)): blue, $D_{glob} = 0$ Å; red, $D_{glob} = 1$ Å; yellow, $D_{glob} \geqslant 2$ Å. Same viewing angle as in Figure 1(a).

As a basis for the following discussion on implications of the present, new results for mechanistic aspects of ligand binding by CypA and of intermolecular recognition between the CypA-CsA complex and CaN, we use a review of the data up to 1994 by Braun *et al*. (1995) and the analysis of the high-resolution X-ray crystal structure of free human CypA by Ke (1992).

In the complexes with CsA and other ligands, CypA forms a Y-shaped binding pocket that in-

Table 2. Analysis of the 20 best DIANA conformers of free cyclophilin A after restrained energy minimization with the program OPAL

Quantity	Average value± standard deviation	Range
DIANA target function (Å^2)[a]	4.96 ± 0.60	3.95 . . . 5.86
AMBER-energy (kcal/mol)	−7216 ± 113	−7440 . . . −6993
Residual NOE distance constraint violations (Å)		
Sum	17.8 ± 0.6	16.5 . . . 18.8
Maximum	0.10 ± 0.01	0.09 . . . 0.11
Residual dihedral angle constraint violations (deg.)		
Sum	20.0 ± 5.1	9.0 . . . 30.3
Maximum	2.1 ± 0.2	1.4 . . . 2.5
RMSD values calculated for different atom selections (Å)[b]		
Backbone atoms N, C^α, C′ (2–165)	0.49 ± 0.05	0.42 . . . 0.58
All heavy atoms (2–165)	0.88 ± 0.05	0.77 . . . 0.95
Backbone atoms of regular secondary structures[c]	0.32 ± 0.04	0.26 . . . 0.39
Best-defined backbone segments[d]	0.36 ± 0.04	0.30 . . . 0.43
Same + best-defined side-chains[e]	0.38 ± 0.04	0.32 . . . 0.45
Backbone (2–165) + well defined side-chains[f]	0.57 ± 0.04	0.50 . . . 0.67

[a] Before energy minimization.

[b] Averages and standard deviations are given for the pairwise RMSD values between each of the 20 energy-refined DIANA conformers and the mean structure. The numbers in parentheses denote the polypeptide segments considered in the comparison.

[c] The following 76 residues are part of regular secondary structures: 5 to 12, 15 to 24, 53 to 57, 61 to 64, 97 to 100, 112 to 115, 127 to 134, 156 to 163 (β-strands) and 30 to 41, 120 to 122, 136 to 145 (helices).

[d] Best-defined backbone segments are those for which each individual residue has a global displacement smaller than 0.5 Å, which holds for the following 126 residues: 3 to 43, 47 to 49, 53 to 63, 78 to 79, 82-83, 86 to 101, 107 to 122, 126 to 147, 150 and 152 to 164.

[e] Best-defined side-chains are those with global displacements smaller than 0.5 Å and include the following 71 residues: 4 to 7, 10-11, 14, 16 to 18, 20, 24, 26, 29-30, 32-33, 38-39, 41-42, 45, 47, 50, 56 to 59, 64-65, 72, 74-75, 78, 80, 90, 92 to 98, 101, 104, 107, 109, 113 to 117, 119, 122, 124, 127 to 130, 132, 135, 138-139, 141-142, 145-146, 150, 159, 162 and 164.

[f] Well-defined side-chains are those with global displacements smaller than 1.0 Å and include the following 120 residues: 3 to 14, 16 to 18, 20 to 22, 24 to 27, 29 to 33, 35-36, 38 to 42, 44 to 47, 50-51, 53, 56 to 62, 64-65, 67, 72, 74-75, 77-78, 80, 83, 87 to 90, 92- 105, 107, 109-110, 112 to 119, 121-122, 124, 126 to 130, 132-133, 135 to 139, 141 to 143, 145 to 147, 150, 152 to 154, 156 to 159 and 161 to 164.

Table 3. Experimental ^{1}H chemical shifts of amino acid side-chains and ring current effects in CypA

Assignment[a]			$\Delta\delta(^1H)$[a] (ppm)	Ring current shift[b] min…max (ppm)	Comments
19	Arg	H^{ε}	1.82	−0.46…0.18	Salt bridge
22	Phe	H^{ε}	−1.24	−1.75…0.60	
31	Lys	$H^{\varepsilon 3}$	−1.17	−0.61…−0.02	
35	Asn	$H^{\delta 21}$	1.35	−0.24…0.36	Hydrogen bond
36	Phe	H^{ε}	−1.83	−3.81…0.60	
37	Arg	H^{ε}	1.70	−0.06…0.04	Salt bridge
39	Leu	$H^{\beta 3}$	−1.98	−2.25…0.16	
61	Met	H^{γ}	−1.63	−2.35…0.28	
66	Asp	$H^{\beta 3}$	−1.05	−0.74…0.16	
76	Lys	$H^{\varepsilon 3}$	−1.49	−1.59…−0.08	
78	Ile	$H^{\gamma 13}$	−1.66	−3.03…0.17	
98	Leu	$H^{\beta 2}$	−1.50	−0.95…−0.08	
98	Leu	$H^{\beta 3}$	−1.57	−1.84…−0.34	
98	Leu	H^{γ}	−1.24	−0.85…0.33	
98	Leu	$H^{\delta 1}$	−1.12	−3.38…0.33	
98	Leu	$H^{\delta 2}$	−1.49	−4.49…0.02	
99	Ser	$H^{\beta 3}$	−1.00	−1.90…0.35	
108	Asn	$H^{\beta 2}$	−1.29	−2.35…0.23	
108	Asn	$H^{\beta 3}$	−1.84	−3.01…0.10	
108	Asn	$H^{\delta 22}$	−1.20	−4.53…0.14	
112	Phe	$H^{\varepsilon 1}$	−1.20	−2.39…0.53	
119	Thr	H^{β}	−1.41	−2.76…−1.09	
119	Thr	$H^{\gamma 1}$	−2.81	−3.28…0.17	
122	Leu	$H^{\beta 2}$	−1.55	−2.52…−0.34	
122	Leu	H^{γ}	−1.28	−1.97…−0.15	
129	Phe	$H^{\varepsilon 1}$	−1.75	−3.50…0.30	
158	Ile	$H^{\delta 1}$	−1.02	−3.89…0.26	

[a] All side-chain protons with a deviation of the chemical shift relative to the random coil value (Wüthrich, 1986), $\Delta\delta(^1H)$, larger than 1.0 ppm are listed.

[b] Minimal and maximal value among the 20 energy-minimized conformers used to represent the NMR structure. For geminal protons without stereospecific assignments the values are listed that give the better fit with the experiment.

Table 4. Survey of published three-dimensional cyclophilin structures

Reference	Ligand, comments	Method	PDB entry
Cyclophilin A			
Kallen *et al.* (1991); Kallen & Walkinshaw (1992)	Acetyl-Ala-Ala-Pro-Ala-amidomethyl-cumarine	X-ray/NMR	–[a]
Spitzfaden *et al.* (1992)	CsA	NMR/X-ray[b]	–
Ke *et al.* (1991); Ke (1992)	–	X-ray	2CPL
Pflügl *et al.* (1993, 1994)	CsA (decamer)	X-ray	–[a]
Mikol *et al.* (1993)	CsA (monomer)	X-ray	1CWA
Ke *et al.* (1993a)	Ala-Pro	X-ray	2CYH
Thériault *et al.* (1993)	CsA	NMR	–
Mikol *et al.* (1994a)	[4-[(E)-2-Butenyl]-4,4,*N*-trimethyl-L-threonine][1]-cyclosporin	X-ray	1CWB
Ke *et al.* (1994)	CsA	X-ray	2RMA
Ke *et al.* (1994)	*N*-Methyl-4-[(E)-2-butenyl]-4,4-dimethylthreonine-cyclosporin	X-ray	2RMB
Papageorgiou *et al.* (1994)	(4,*N*-Dimethylnorleucine)-4-cyclosporin	X-ray	1CWC
Spitzfaden *et al.* (1994)	CsA	NMR	3CYS
Mikol *et al.* (1995)	(5-Hydroxynorvaline)-2-cyclosporin	X-ray	1MIK
Zhao & Ke (1996a)	Succinyl-Ala-Ala-Pro-Phe-nitroanilide	X-ray	1RMH
Zhao & Ke (1996b)	Ser-Pro, His-Pro, Gly-Pro	X-ray	3–5CYH
Gamble *et al.* (1996)	CypA-HIV-1 capsid (1-151)	X-ray	–
Zhao *et al.* (1997)	CypA-HIV-1 gag capsid (81-105)	X-ray	1FGL
Other cyclophilins			
Ke *et al.* (1993b)	Murine CypC-CsA complex	X-ray	2RMC
Mikol *et al.* (1994b)	CypB-CsA complex	X-ray	1CYN
Clubb *et al.* (1994)	*E. coli* Cyp	NMR	1CLH
Konno *et al.* (1996)	*E. coli* Cyp–succinyl-Ala-Pro-Ala-*p*-nitroanilide complex	X-ray	1LOP

[a] The coordinates have been obtained directly from the authors.

[b] Molecular model of the CypA–CsA complex based on the NMR structure of CypA-bound CsA (Weber *et al.*, 1991), the X-ray structure by Kallen *et al.* (1991), and measurements of intermolecular CypA-CsA NOEs in the complex.

cludes four strands of the β-barrel, with residues 53 to 57, 61 to 64, 97 to 100 and 112 to 115, and four loops with residues 65 to 75, 102 to 110, 117 to 128 and 147 to 150. While the four β-strands belong to the most precisely defined parts of the molecular structure, the loops surrounding the binding pocket display significantly increased structural disorder. For the high-resolution crystal structure of free CypA, Table 5 of Ke (1992) lists a total of 28 lattice contacts; among these, seven involve residues of ligand binding-site loops in both molecules, and 18 involve a binding-site loop residue and one a binding-site β-strand residue in one of the two interacting molecules. Overall, the ligand-binding site of CypA is clearly prone to be affected by packing effects in the single crystals, and thus the NMR solution structure of CypA fills an important gap in providing a reference for assessment of structural changes upon ligand binding to CypA. The following detailed comparisons of the CypA structures in solution and in crystals, and of free CypA in solution with CypA conformations in different complexes imply that the three-dimensional polypeptide fold of CypA, which is faithfully maintained throughout the structures of Table 4, serves as a scaffold that supports subtle conformational variations in and around the ligand-binding site.

The high quality of the NMR structure determination of CypA warrants a detailed analysis of local structural features. On the basis of more than 99.5% completeness of the sequence-specific assignments of the aliphatic protons, the aromatic protons and the backbone amide protons (Table 1), the NOESY spectra yielded 4101 meaningful upper distance constraints (Table 1). (There remained, nonetheless, peaks in the NOESY spectra that could not be unambiguously assigned because they correspond to two or several overlapped NOE cross-peaks). For comparison, one would expect 4053 meaningful NOE distance constraints from the assumption that NOEs are observable for all pairs of protons, or groups of equivalent protons, that are less than 4.6 Å apart in all 20 DIANA conformers. This extensive data set is highly self-consistent, as evidenced by the convergence behavior and the low residual target function values in the structure calculations (Table 2).

Comparison of the solution and crystal structures of free CypA

The global RMSD calculated for the backbone atoms N, C^{α} and C' of the regular secondary structures in the mean NMR solution structure and the X-ray crystal structure (Ke, 1992) is 0.49 Å, and the positions of the backbone atoms coincide within the precision of the two structure determinations. In addition to the chain ends, significant backbone differences in the entire polypeptide chain are limited to residues 42 to 46, 67 to 75, 79 to 81, 120 to 124 and 148 to 149 (Figure 3(c)). Most of these residues are located within or near loops that constitute the CsA binding pocket. In the NMR structure these loops are displaced towards the free space of the binding pocket (Figure 5(a)). The most pronounced shift of about 1.5 Å is observed for the loop of residues 67 to 75, which is probably due to crystal contacts at the molecular interface: the residues 67 to 71 are involved in four out of a total of six intermolecular hydrogen bonds, i.e. Phe67 O′–$HN^{\delta 2}$ Asn137, Thr68 O′–HN Arg19, Arg69 $N^{\eta 2}H$–O^{δ} Asp9 (salt bridge), and His70 $N^{\varepsilon 2}H$–O, Arg19 (Figure 5(b)). In the NMR structure the loop formed by residues 67 to 75 is less precisely defined and displays increased mobility when compared to the rest of the protein (see below).

Figure 5(c) and (d) afford a visual impression of the close correlation between corresponding side-chains in the NMR and crystal structures. There are only a small number of side-chains with significantly different conformations in the two structures, i.e. with $D^{sc}_{glob} \geqslant 2.0$ Å and $D^{sc}_{glob} \geqslant 1.0$ Å: Val2, Glu15, Lys31, Tyr48, His54, Arg55, Arg69, His70, Glu81, Lys82, Glu140, Arg144, Arg148, Lys151 and Glu165. With the only exceptions of Val2 near the N terminus and Tyr48, which is completely shielded from solvent contact and for which NMR constraints are scarce because of dynamic line broadening (see above), all these positions contain charged, long side-chains that are solvent-exposed and poorly defined in the NMR structure and have high temperature factors in the crystal structure (Figure 3).

Comparison of CypA in the free state and in complexes with different ligands

The different CypA structures studied so far with and without bound ligands, in solution and in different crystal forms, are all very similar. The average pairwise RMSD values between all available structures of ligated human CypA (Table 4; for the NMR structure from Spitzfaden *et al*. (1994), only the mean coordinates were considered) are 0.30 Å for the backbone atoms and 0.87 Å for all heavy atoms of residues 2 to 165. The mean of the pairwise global displacements per residue of the backbone heavy atoms, D^{bb}_{glob}, in these structures relative to the mean coordinates calculated after superposition of the backbone heavy atoms of residues 2 to 165 for minimal RMSD are, on average, below 0.15 Å. Except for the chain ends, only the residues 13 to 16, 27, 44-45, 69 to 72, 80-81, 134 and 144 to 155 have a D^{bb}_{glob} >0.20 Å, which coincides very closely with the locations of the less well defined regions in unligated CypA (Figure 3 (b) and (d)). With respect to the mean NMR structure, a very similar picture to that described for the crystal structure of CypA in the free state (Ke, 1992) emerges. The regular secondary structures of the mean NMR structure as defined in Table 2 are superimposable with all other CypA-ligand structures with a mean pairwise RMSD of 0.50 Å for the backbone heavy atoms. Larger differences, with D^{bb}_{glob} >1.0 Å, are found only for residues 42 to 46,

69 to 75, 81, 121-122 and 146 to 148, and for the chain ends. Most of these residues are involved in ligand binding (see above).

Hydrogen bonds, conformational equilibria and internal mobility

Dynamic features of CypA in solution and, for the purpose of comparison, of the CypA-CsA complex in solution were investigated from measurements of proton exchange rates, line shapes and chemical shift effects, relaxation times, slow inversion of aromatic rings in the core of the β-barrel, and the local precision of discrete polypeptide segments in the three-dimensional structure.

The pattern of backbone amide proton exchange rates, k_{NH}, fits nicely with the hydrogen bonds observed in the NMR structure (Figure 6). Nearly all amide protons with $k_{NH} < 10^{-3}$ min^{-1} are involved in backbone–backbone hydrogen bonds in at least ten of the 20 NMR conformers as well as in the crystal structure (Figure 6(b)). Exceptions are Phe60, Ile97, Ala14 and Ile158; however, if the criterion for the identification of a hydrogen bond is loosened to a maximal proton-acceptor distance of 3.0 Å (instead of 2.4 Å) and a maximal angle of 50° (instead of 35°) between the donor-proton bond and the line connecting the donor and acceptor heavy atoms, hydrogen bonds are assigned also for these amide protons in the NMR structure. Three highly conserved backbone–backbone hydrogen bonds with slow exchange of the corresponding amide protons ($k_{HD} < 10^{-3}$ min^{-1}) are located outside of regular secondary structures: Val29 NH–O′ Phe25 is in a helix-like turn. Tyr48 NH–O′ Leu39 stablizes the C-terminal turn of the first α-helix, and Ser51 NH–O′, Tyr48 is part of a β-turn. Rapidly exchanging amide protons that are involved in a backbone-backbone hydrogen bond in more than 10 of the 20 NMR conformers and in the crystal structure are observed for Asp13, Gly45, Ser77, Lys125, Gly150, Ser153 and Leu164 (Figure 6). However, these hydrogen bonds are not part of regular secondary structures, and in all instances the amide protons are close in space to a charged or polar group that might catalyze the exchange. Some amide protons involved in backbone to side-chain hydrogen bonds also show slowed exchange: Lys31 and Thr32, which combine with the carboxylate group of Glu86 to form a well defined ''long-range N-cap'' of the first α-helix (Figure 5(c)), Asp27, Glu43, Gly75, Ile78, Tyr79, Asp85, Ile89

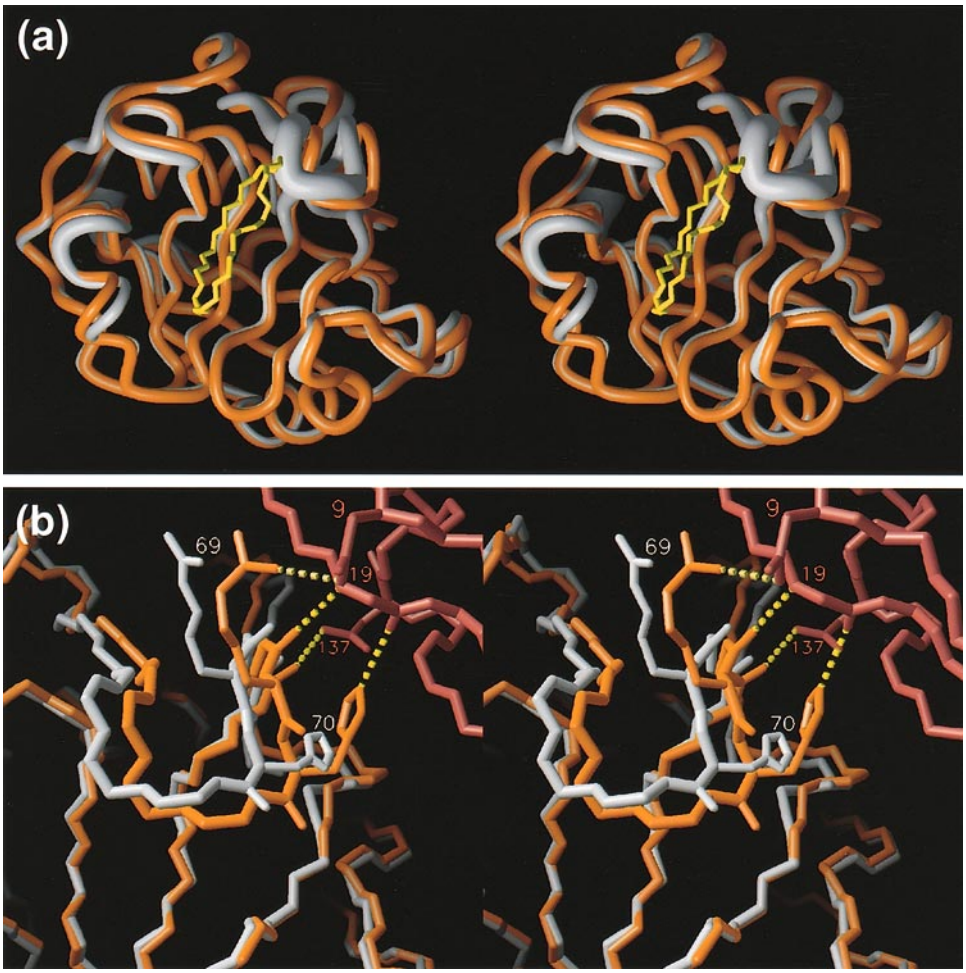

Figure 5. *(legend opposite)*

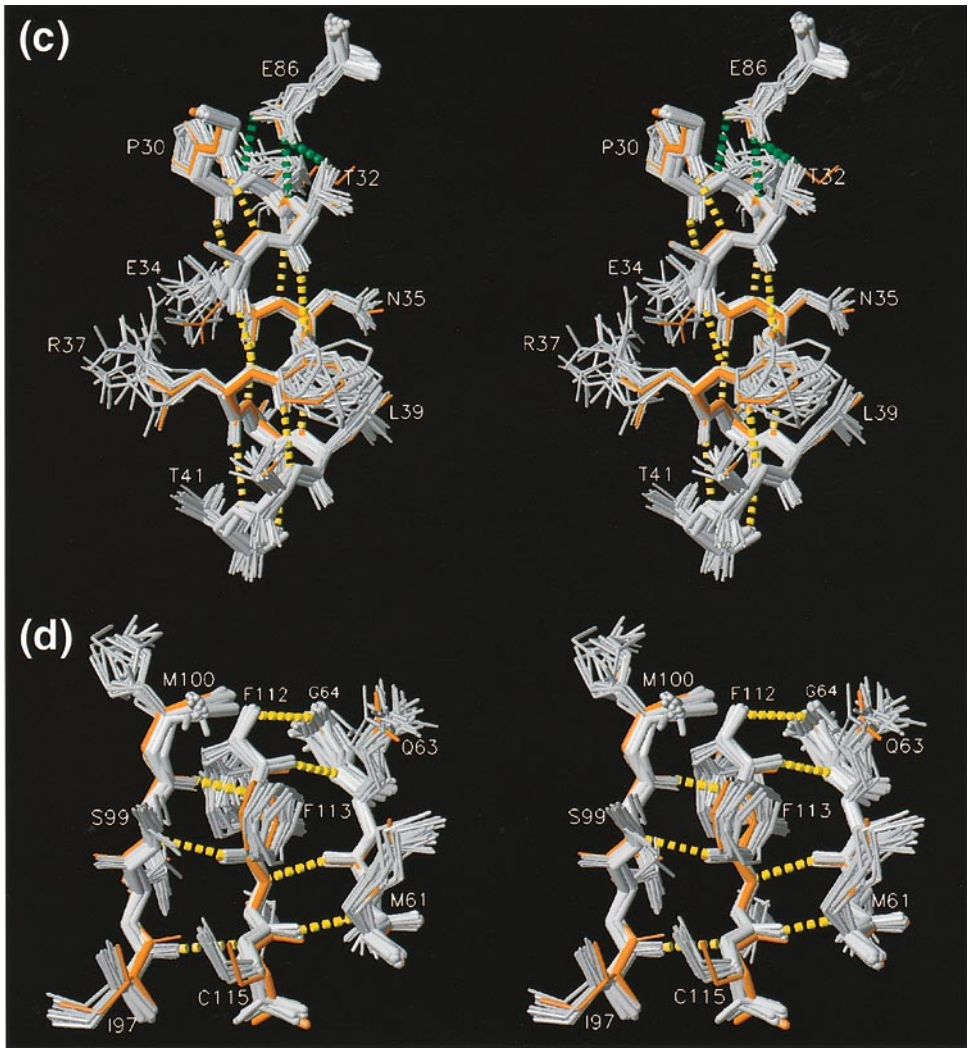

Figure 5. Comparison of the NMR solution structure and the X-ray crystal structure (Ke, 1992) of free CypA. (a) Stereo view of the polypeptide backbones after superposition for minimal RMSD between the heavy atoms N, C^{α} and C′ of residues 2 to 165. A spline function was drawn through the C^{α} positions. In the NMR structure (gray) the radius of the cylindrical rod corresponds to the mean of the global displacements, D^{bb}_{glob} (Figure 3(b)), among the 20 energy-minimized NMR conformers, and in the crystal structure (orange) to the converted temperature factors, $\sqrt{B/8\pi^2}$, of the C^{α} atoms. In addition, the position of CsA (yellow) in the NMR structure of the CypA–CsA complex (Spitzfaden *et al.*, 1994) is shown, as obtained after superposition of the backbone heavy atoms N, C^{α} and C′ of residues 2 to 165 of CypA in the complex and in the free form for minimal RMSD. (b) Stereo view of the crystal contacts in the loop containing His70. The backbone and selected side-chains of the mean NMR structure (gray) and the crystal structure (orange) are shown after superposition of the backbone heavy atoms N, C^{α} and C′ of residues 2 to 165 for minimal RMSD. A neighboring CypA molecule in the crystal lattice is shown in dark red. Intermolecular hydrogen bonds and salt bridges between the neighboring CypA molecules in the crystal lattice are indicated with yellow broken lines. Numbers indicate the sequence positions of selected residues. (c) Stereo view of a heavy-atom representation of residues 29 to 41 and Glu86 after local superposition of the backbone heavy atoms N, C^{α} and C′ for minimal RMSD. The 20 DIANA conformers representing the NMR solution structure are shown in gray, and the crystal structure in orange. The residues shown form the first α-helix (residues 30 to 41) and a long-range N-cap. Helical and N-capping hydrogen bonds are represented with yellow and green broken lines, respectively (see the text for further details). (d) Stereo view of a heavy-atom representation of β-strands 4, 5 and 6 comprising residues 61 to 64, 97 to 100 and 112 to 115, respectively, after local superposition of the backbone heavy atoms N, C^{α} and C′ for minimal RMSD. Coloring as in (c), with the hydrogen bonds between the strands represented with yellow broken lines.

and Cys161. Overall, slow amide proton exchange correlates well with high local precision of the NMR structure determination (Figure 1(d)). Note that the β-strand with residues 53 to 57 has rather fast amide proton exchange rates (see also Figure 6(a)), indicating a zipper-like function for the β-barrel that would allow conformational ''breathing'' of the interior side-chains.

In free CypA the average half-widths at half-height of the amide proton NMR lines at 26°C are

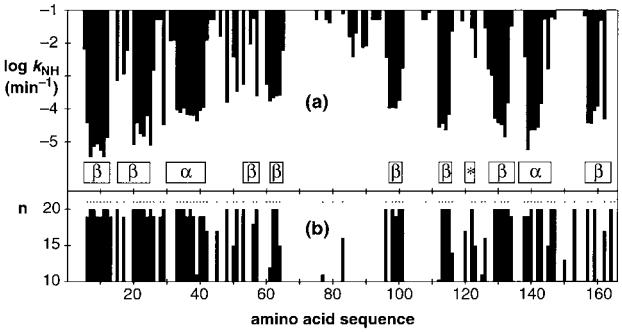

Figure 6. (a) Plot *versus* the amino acid sequence of the exchange rates with solvent ^2H_2O, k_{NH}, for the backbone amide protons of free CypA at pD 6.5 and 26°C. The locations of the regular secondary structure elements are given at the bottom, where α, * and β indicate α-helix, 3_{10}-helix and β-strand, respectively. (b) Plot of the numbers among the 20 energy-minimized DIANA conformers for which the individual amide protons are involved in a backbone-backbone hydrogen bond. Dots at the top indicate that a corresponding hydrogen bond was also identified in the crystal structure (Ke, 1992). The criteria used for the identification of a hydrogen bond are a maximal proton to acceptor distance of 2.4 Å and a maximal angle of 35° between the donor-proton bond and the line connecting the donor and acceptor heavy atoms (Levitt, 1983).

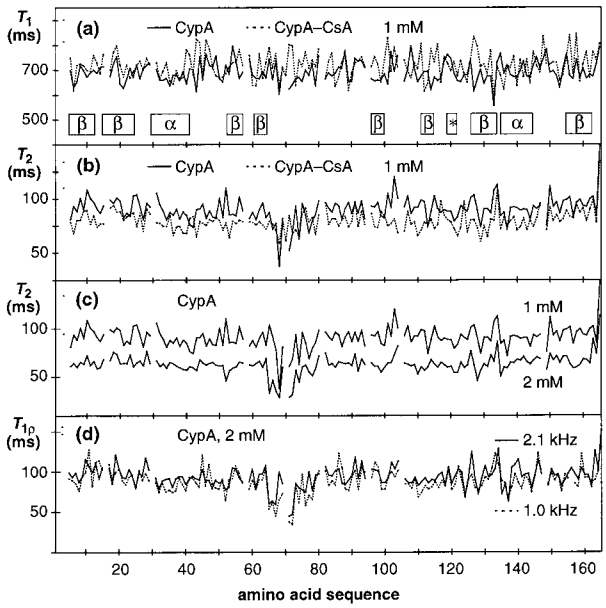

Figure 7. Plots of backbone ^{15}N spin relaxation times of free and complexed CypA *versus* the amino acid sequence. (a) Longitudinal relaxation time, T_1, of free CypA (continuous line) and CsA-complexed CypA (dotted line); (b) transverse relaxation time, T_2, of free CypA (continuous line) and complexed CypA (dotted line); (c) transverse relaxation time, T_2, of free CypA at 1 mM and 2 mM concentration; (d) transverse relaxation time in the rotating frame, $T_{1\rho}$, of free CypA at 2 mM concentration at 1.0 (dotted line) and 2.1 kHz (continuous line) spin lock power. The locations of the regular secondary structure elements are given in (a), where α, * and β indicate α-helix, 3_{10}-helix and β-strand, respectively.

about 7.5 Hz. For the residues 52, 65 to 72 and 81 the lines are broadened by at least 5 Hz, so that the corresponding cross-peaks in 2D and 3D NMR spectra appear much weaker than the other signals. At lower temperatures the line broadening is stronger and some of the peaks are no longer observable, whereas at higher temperatures they get sharper and more intense. This indicates that the loss of signal intensity is related to conformational exchange on the millisecond time-scale. In the CypA-CsA complex no such line broadening is observed, and the chemical shifts of these amide protons differ significantly between the free and the complexed protein.

The aforementioned data on local conformational equilibria were complemented by information on the frequencies of associated rate processes, obtained from T_1 and T_2 spin relaxation times for ^{15}N in free CypA and in the CypA-CsA complex, and $T_{1\rho}$ in CypA (Figure 7). We also measured T_1 and T_2 for ^{15}N with two different CypA concentrations, i.e. 1 mM and 2 mM (Figure 7(c)). The change in viscosity at the different concentrations caused a systematic decrease in the T_2 values of the more highly concentrated sample by about 28 ms (Figure 7(c)). Apart from that, the most obvious difference is found for residues 52 and 65, which are exchange broadened (see above) and have very low signal-to-noise ratios in the 1 mM sample. Nevertheless, the RMSDs between the T_1 and T_2 values after correction for these systematic differences are only 50 ms and 9 ms, respectively. This indicates random uncertainties (standard deviations) for the T_1 and T_2 values of CypA presented in Figure 7 of about 35 ms and 6.4 ms, respectively.

From the T_1/T_2 ratio of the residues in regular secondary structures, overall rotational correlation times, τ_R, of approximately 8.2 ns and 9.1 ns were obtained for free CypA and the CypA-CsA complex, respectively, using the assumption that the protein reorients isotropically in solution. In general, T_1 and T_2 values are rather homogeneous throughout the polypeptide chains, and significant differences between the free and complexed forms of CypA are observed only for two fragments involved in CsA binding. For residues 68 to 72 the T_2 values are reduced in the free protein, which presumably manifests the conformational exchange that causes the aforementioned line broadening. For residues 101 to 104, longer T_2 values indicate higher internal mobility in the free protein (Figure 7(b)). The fact that $T_{1\rho}$ of residues 65 to 72 could only partially be increased at relatively high spin lock fields of 2.1 kHz (Figure 7(d)) allows us to establish a limit of about 0.1 to 1 ms for the effective correlation time, which we assign to this conformational exchange (Szyperski *et al.*, 1993).

The 20 NMR conformers include two different conformations for the peptide bond Arg69-His70 which interconvert by simultaneous rotation of ψ_i and ϕ_{i+1} by about 180° (Figure 8(a)). The rate of interconversion is sufficiently slow to cause the appearance of separate ^1H-^{15}N peaks for the different conformations (Figure 8(b)). The two groups of conformations I and II show the expected intraresidual and sequential NOEs. The chemical shifts of conformation I could be unambiguously assigned by sequential and intraresidual NOEs. These shifts are nearly identical with those of the CypA-CsA complex (Spitzfaden *et al.*, 1994). In this context it is interesting that the crystal structure of free CypA and the structures of all known CypA-ligand complexes (Table 4) contain the conformation I. For conformation II two possible chemical shifts are found for the NH group, both showing sequential NOEs to the amide proton of Asn71 (Figure 8(b)). Since the sequential d_{NN}^{II} NOEs, which correspond to a distance of about 2.0 Å (green dotted line in Figure 8(a)), are only very weak, the intraresidual $d_{N\alpha}^{II}$ NOE, which would correspond to a distance of about 2.9 Å, may escape detection.

Implications from the dynamic properties of CypA for ligand binding and calcineurin recognition

The characterization of dynamic properties of proteins by NMR supplements the static picture of a three-dimensional structure with a time-resolved, dynamic view. It is common knowledge that proteins may undergo conformational changes to allow binding of ligands, substrates or receptors. Similarly, the observed flexibility in the CsA-binding region of free CypA seems to be necessary to allow access of ligands to the active site located on the bottom of a deep binding pocket and to promote tight binding. Perhaps even more important, the implicated flexibility could, at least in part, be responsible for the relative substrate promiscuity of CypA. It appears to be in line with this hypothesis that the flexible polypeptide fragments are preferentially involved in packing contacts in CypA crystals (Figure 5(b)). These observations clearly extend earlier conclusions based on crystal structures of free CypA and CypA complexes, which proposed that CypA has a rather rigid CsA-binding surface representing a preformed near-ideal CsA-binding cavity (Altschuh *et al.*, 1994). The interaction with CsA, however, leads to a stabilization of the mobile loops surrounding the CsA binding pocket (Figure 5(a)), which probably also causes a higher temperature stability of the complex than for free CypA.

Our findings are consistent with the results obtained previously from analogous studies performed with the FKBP12/FK506 system (Cheng *et al.*, 1993, 1994). The available evidence indicates that the immunophilin-immunosuppressant complex binds as a rather rigid structural entity to CaN. When considering the enthalpic cost, formation of the ternary complex is unlikely to involve major structural changes of the preformed

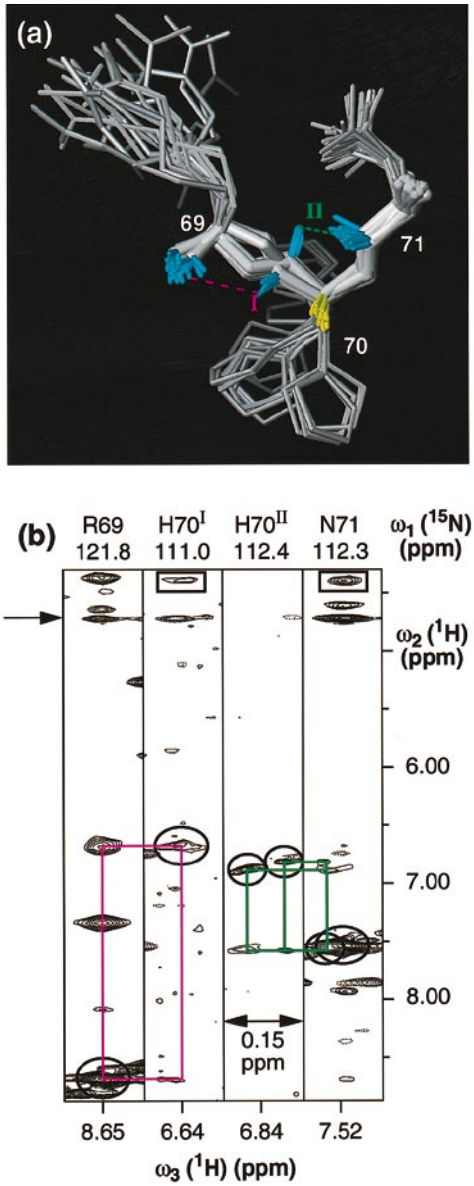

Figure 8. Conformational exchange at His70 in free CypA. (a) Heavy-atom representation of the polypeptide backbone fragment of residues 69 to 71 of the 20 energy-minimized DIANA conformers after local superposition of the backbone heavy atoms N, C^α and C' for minimal RMSD. Additionally, all N-H bonds and the C^α-H bond of His70 are shown in blue and in yellow, respectively, and short d_{NN} distances belonging to the local conformations (I) and (II) are shown with broken lines in magenta and green, respectively. (b) Contour plots of [$\omega_2(^1H)$, $\omega_3(^1H)$] strips from the 3D ^{15}N-resolved [^1H, ^1H]-NOESY spectrum of CypA (2 mM in 90% H_2O/10% ^2H_2O, pH 6.5, at 26°C, ^1H resonance frequency = 750 MHz, $\tau_m = 60$ ms). Direct peaks are circled, the sequential d_{NN} connectivities in the His70 conformations (I) and (II) are represented by magenta and green lines, respectively, and NOEs to His70 H^α are shown in rectangular boxes. On the left side of the Figure an arrow indicates the chemical shift position of the water signal (4.74 ppm).

binding interface of the immunophilin-immunosuppressant complex (see also Cheng *et al*., 1994). This view is supported by the fact that neither FKBP12 nor CaN in the crystal structure of the ternary CaN-FK506-FKBP12 complex (Kissinger *et al*., 1995) revealed differences with respect to the free proteins that would be detectable at a crystallographic resolution of 3.5 Å. Similarly, the binding interactions in the structure at 2.5 Å resolution of a ternary complex containing a proteolytic fragment of bovine CaN and the FKBP12-FK506 complex appears to involve only subtle conformational changes in the FKBP12-FK506 binding interface (Griffith *et al*., 1995).

Structural homology of CypA with domain II of the *E. coli* DNA topoisomerase I

From comparison of the crystal structure of CypA with other proteins containing either antiparallel or parallel eight-stranded β-barrel supersecondary structures, Ke (1992) concluded that, in spite of some obvious structural similarities, the (+1, −3, −1, −2, +1, −2, −3) topology of CypA is unique among the members of the β-barrel family of proteins. In a further search for structural similarities between CypA and other protein structures in the Brookhaven Protein Data Bank, the distance matrix algorithm implemented in the program DALI (Holm & Sander, 1993) revealed only one protein with close topological similarity outside of the Cyp family, namely the domain II of *Escherichia coli* DNA topoisomerase I (Lima *et al*., 1994). This domain consists of a six-stranded β-barrel with the topology +1, −3, −1, −1, +3. Thus, the two structures coincide in the first four β-strands and the helix between the second and the third strand. Additionally, the spatial arrangement of strands 5 and 6 of the topoisomerase coincides closely with strands 6 and 8 of CypA, and the two proteins are overall very similar. The RMSD for the backbone heavy atoms of 40 residues that represent the major part of the β-barrel (2 to 12, 15 to 21, 51 to 53, 62 to 64, 98 to 100, 111 to 113 and 155 to 164 of CypA, and 218 to 228, 231 to 237, 264 to 266, 415 to 417, 239 to 241, 419 to 421 and 458 to 467 of the topoisomerase domain II) is only 2.0 Å, although the sequence identity of the superimposed residues is only 8%. This unexpected structural similarity may presently be mainly considered to be a curiosity, as there is no further indication of either functional or evolutionary relationship between the two proteins.

Materials and Methods

Sample preparation

Cyclophilin A labeled uniformly with ^{13}C, with ^{15}N, or with both ^{13}C and ^{15}N, was overexpressed in *E. coli*. Cells were grown on 1 or 2 l of Martek CELTONE rich medium containing M9 salts (Sambrook *et al*., 1989). Purification of CypA and the preparation of the CypA-CsA complex were as described (Weber *et al*., 1991). The yield of purified protein was about 35 mg/l. Samples were dialyzed extensively against an optimized NMR-buffer containing 10 mM Na^+/K^+-phosphate (pH 6.5), 100 mM $NaNO_3$, 5 mM [$^2H_{10}$]-1,4-DL-dithiothreitol (DTT) and 50 μM NaN_3.

NMR spectroscopy

NMR measurements were performed on Bruker AMX600 and Varian U750+ spectrometers equipped with four channels, using 2.0 mM CypA samples either in 90% H_2O/10%^2H_2O or in ^2H_2O. Unless stated otherwise the spectra were recorded at pH/pD 6.5 and at 26°C. Quadrature detection in the indirect dimensions was achieved using States-TPPI (Marion *et al*., 1989). For measurements at 600 MHz the water signal was suppressed by spin-lock pulses (Messerle *et al*., 1989), and on the 750 MHz spectrometer pulsed field gradients were used for suppression of undesired coherence pathways and the residual water signal (Bax & Pochapsky, 1992; Wider & Wüthrich, 1993). For data processing and spectral analysis we used the programs PROSA (Güntert *et al*., 1992; Bartels *et al*., 1995a) and XEASY (Bartels *et al*., 1995b), respectively.

Resonance assignments for ^1H, ^{13}C and ^{15}N were obtained from the 13 experiments listed in the upper part of Table 5, which includes the key experimental parameters. Input for the structure calculation was collected using the five experiments at the bottom of Table 5. The three NOESY spectra were all recorded with $\tau_m = 60$ ms at a ^1H resonance frequency of 750 MHz. The total measuring time was about 4.5 days each for the 3D spectra and 20 hours for the 2D spectrum. Vicinal $^3J_{HN\alpha}$ coupling constants were determined by inverse Fourier transformation of in-phase multiplets (Szyperski *et al*., 1992) from a 2D [^{15}N, ^1H]-HSQC spectrum recorded at 750 MHz. The digital resolution after zero-filling was 2.6 Hz/point along ω_1 and 1.3 Hz/point along ω_2. Vicinal $^3J_{N\beta}$ scalar coupling constants were estimated from a 3D *ct*-HNHB spectrum.

For the determination of amide proton exchange rates, a sample containing 450 μl of a 2.0 mM solution of uniformly ^{15}N-labeled CypA was ultrafiltered several times at 4°C against NMR-buffer in ^2H_2O. The 36 2D [^{15}N, ^1H]-HSQC spectra were recorded at 26°C, with the delays between the individual recordings logarithmically distributed over a period of three months. In-between the NMR recordings the sample was kept in a waterbath at 26°C. The rate constants were obtained from a least-squares fit of a single exponential function to the peak volumes.

The ^{15}N spin relaxation measurements were performed with 1 mM solutions of uniformly ^{15}N-labeled CypA, both free and complexed with unlabeled CsA, at a ^1H resonance frequency of 600 MHz, following procedures described by Szyperski *et al*. (1993) and Peng & Wagner (1994). In order to obtain estimates for the random uncertainties, spectra were also recorded with a 2 mM sample of unligated CypA. For the measurement of longitudinal relaxation times, T_1, eight ^{15}N-T_1-modulated 2D [^{15}N, ^1H]-HSQC spectra were recorded with relaxation delays of 10, 100, 200, 400, 600, 800, 1500 and 2500 ms. Transverse relaxation times, T_2, were obtained from 10 ^{15}N-T_2-modulated 2D [^{15}N, ^1H]-HSQC spectra with relaxation delays of 1.7, 10, 20, 30, 40, 60, 80, 120, 160 and 220 ms. Rotating frame relaxation times, $T_{1\rho}$, were calculated from eight ^{15}N-$T_{1\rho}$-modulated 2D [^{15}N,

Table 5. NMR spectra recorded for the resonance assignment and the collection of the input for the structure calculation of CypA

Experiment (τ_m)	Sample[b]	$\nu_0(^1H)$ (MHz)	Data size (complex points)	t_{max} (ms)	Reference
2D [^{15}N, ^{1}H]-HSQC	N, h	600	180 × 1024	84.6 (N), 112.6 (H)	Bodenhausen & Ruben (1980)
2D *ct*-[^{13}C, ^{1}H]-HSQC, carbonyl and aromatic editing	C, d	750	180 × 2048	45.0 (C), 204.8 (H)	Vuister & Bax (1992); Grzesiek & Bax (1993)
3D CBCA(CO)NH	CN, h	600	56 × 40 × 512	6.5 (C), 16.4 (N), 65.6 (H)	Grzesiek & Bax (1992)
3D *ct*-HNCA	CN, h	600	44 × 50 × 512	21.9 (N), 12.3 (C), 65.6 (H)	Madsen & Sørensen (1992)
3D HCCH-TOCSY (5.8, 14.2 ms)	C, d	600	32 × 100 × 512	10.2 (C), 15.9 (H), 65.6 (H)	Bax *et al.* (1990)
3D ^{13}C-res. [^{1}H, ^{1}]-TOCSY (20 ms)	C, d	600	32 × 100 × 512	10.2 (C), 15.9 (H), 65.6 (H)	Edison *et al.* (1991)
3D *ct*-HCCH-COSY	C, d	600	25 × 90 × 512	8.0 (C), 15.0 (H), 65.6 (H)	Ikura *et al.* (1991)
3D CCH-TOCSY (14.2 ms)	C, d	600	32 × 100 × 512	10.2 (C), 9.4 (C), 65.6 (H)	Fogh *et al.* (1995)
2D [^{1}H, ^{1}H]-clean-TOCSY (20 ms)	N, h	750	474 × 1024	71.8 (H), 112.6 (H))	Griesinger *et al.* (1988)
2D HMBC (optimised for Met)	C, d	750	40 × 2048	20.0 (C), 204.8 (H)	Bax *et al.* (1994)
2D $(H^{\beta})C^{\beta}(C^{\gamma}C^{\delta})H^{\delta}$	C, d	750	32 × 2048	8.0 (C), 204.8 (H)	Yamazaki *et al.* (1993)
2D $H^{\beta}(C^{\beta}C^{\gamma}C^{\delta})H^{\delta}$	C, d	750	100 × 2048	12.5 (H), 204.8 (H)	Yamazaki *et al.* (1993)
3D ^{1}H-TOCSY-relayed *ct*-[^{13}C, ^{1}H]-HMQC (20 ms)	C, d	600	78 × 32 × 1024	16.3 (C), 16.1 (H), 149.5 (H)	Zerbe *et al.* (1996)
3D ^{15}N-res. [^{1}H, ^{1}H]-NOESY (60 ms)[a]	N, h	750	32 × 180 × 512	12.5 (N), 22.1 (H), 46.5 (H))	Fesik & Zuiderweg (1988)
3D ^{13}C-res. [^{1}H, ^{1}H]-NOESY (60 ms)[a]	C, d	750	32 × 180 × 1024	8.2 (C), 22.1 (H), 93.1 (H)	Ikura *et al.* (1990)
2D [^{1}H, H^1]-NOESY (60 ms)	N, h	750	512 × 2048	51.2 (H), 170.6 (H)	Anil-Kumar *et al.* (1980)
3D *ct*-HNHBL[a]	N, h	600	32 × 160 × 512	15.0 (N), 26.7 (H), 60.4 (H)	Archer *et al.* (1991)
2D [^{15}N, ^{1}H]-HSQC (for $^3J_{HN\alpha}$)[a]	N, h	750	256 × 2048	96.3 (N), 186.1 (H)	Bodenhausen & Ruben (1980)

[a] These spectra were used to derive the constraints for the structure calculation.

[b] C and N denote ^{13}C and ^{15}N labeling, respectively, and h denotes the solvent 90% H_2O/10% ^2H_2O, and d the solvent 99.5% ^2H_2O, respectively. Protein concentration ≈2 mM, temperature 26°C, NMR buffer (100 mM $NaNO_3$, 10 mM Na^+/K^+ phosphate, 5 mM [$^2H_{10}$]-1,4-DL-dithiothreitol (DTT), 50 mM NaN_3, pH/pD 6.5).

^{1}H]-HSQC spectra using relaxation delays of 10, 20, 30, 40, 60, 80, 120 and 160 ms. Two different sets of $T_{1\rho}$ experiments were performed, with spin-lock powers of 1.0 and 2.1 kHz, respectively. The spin relaxation times were evaluated using least squares fits of single exponential functions to the experimental data.

Determination of the three-dimensional structure

The input for the distance geometry calculations with the program DIANA consisted of upper distance limits derived from NOESY cross-peak intensities with the program CALIBA (Güntert *et al*., 1991), and of dihedral angle constraints derived from $^3J_{HN\alpha}$ and $^3J_{N\beta}$ coupling constants and intraresidual and sequential NOEs (Wüthrich, 1986) using the program HABAS (Güntert *et al*., 1989, 1991). Before the start of the structure calculations, stereospecific assignments for the isopropyl methyl groups of all Val and Leu were obtained by biosynthetically directed fractional ^{13}C labeling (Senn *et al*., 1989; Neri *et al*., 1989), and HABAS provided a number of stereospecific assignments for β-methylene protons. From comparison of the chemical shifts, the patterns of backbone-backbone NOEs and the amide proton exchange rates in CypA and the CypA-CsA complex there was a clear indication that the 3D structures of free and ligated CypA are closely similar (Spitzfaden *et al*., 1992; Wüthrich, 1986). Therefore, an initial set of NOESY cross-peak assignments were generated by reference to CypA in the 22 conformers used to represent the NMR solution structure of the CypA-CsA complex (Spitzfaden *et al*., 1994). To be on the safe side, only those NOESY signal assignments were accepted for which the corresponding proton–proton distance was smaller than 4.5 Å in all of the 22 conformers of CypA-CsA and for which there was no other assignment possibility within a radius of 6.0 Å. The calculation of the resulting initial structures for unligated CypA was followed by several rounds of structure calculations with DIANA (Güntert *et al*., 1991) and NOESY cross-peak assignment with the program ASNO (Güntert *et al*., 1993). Additional stereospecific assignments were obtained in the course of the structure refinement using the program GLOMSA (Güntert *et al*., 1991). No additional constraint, e.g. to secure the formation of hydrogen bonds, was introduced at any stage of the structure determination.

The final round of DIANA structure calculations was started with 50 randomized conformers and included six REDAC cycles (Güntert & Wüthrich, 1991), for which the maximal target function values per residue for locally acceptable segments were set to 1.0, 0.7, 0.4, 0.4, 0.15 and 0.1 Å^2, respectively. To exclude possible bias by the redundant dihedral angle constraints, minimizations using only the experimental distance and dihedral angle constraints were included after the third, fourth, fifth and sixth REDAC cycles. The 20 DIANA conformers with the smallest target function values (Table 2) were subjected to restrained energy minimization using the AMBER all-atom force field (Weiner *et al*., 1986) as implemented in the program OPAL (Luginbühl *et al*., 1996). The pseudoenergy terms for distance constraints and dihedral angle constraints (Billeter *et al*., 1990) were calibrated such that violations of 0.10 Å and 2.5°, respectively, corresponded to an energy penalty of $k_BT/2$ at room temperature. The restrained energy minimization was carried out in a shell of water molecules with a minimal thickness of 6 Å, performing a total of 1500 steps of conjugate gradient minimization for each conformer. The dielectric constant was 1, and no cutoff for non-bonded interactions was applied. The resulting 20 energy-refined conformers are used to represent the solution structure of CypA. RMSD calculations and color Figures were done with the program MOLMOL (Koradi *et al*., 1996).

Acknowledgments

We thank Dr K. Memmert (Sandoz) for assistance during the production of labeled CypA, and Drs U. Hommel, J. Kallen, H. Widmer, M. Zurini (Sandoz) and P. Luginbühl (ETHZ) for helpful discussions on various aspects of cyclophilin structure and function. Financial support was obtained from Sandoz Pharma AG, Basel, and the Schweizerischer Nationalfonds (project 31.32033.91). We thank Mrs R. Hug for the careful processing of the manuscript.

References

Altschuh, D., Braun, W., Kallen, J., Mikol, V., Spitzfaden, C., Thierry, J. C., Vix, O., Walkinshaw, M. D. & Wüthrich, K. (1994). Conformational polymorphism of cyclosporin A. *Structure,* **2**, 963–972.

Anil-Kumar, Ernst, R. R. & Wüthrich, K. (1980). A two-dimensional nuclear Overhauser enhancement (2D NOE) experiment for the elucidation of complete proton-proton cross relaxation networks in biological macromolecules. *Biochem. Biophys. Res. Commun.* **95**, 1–6.

Archer, S. J., Ikura, M., Torchia, D. A. & Bax, A. (1991). An alternative 3D NMR technique for correlating backbone ^{15}N with side chain H$^{\beta}$ resonances in larger proteins. *J. Magn. Reson.* **95**, 636–641.

Bartels, C., Güntert, P. & Wüthrich, K. (1995a). IFLAT - a new automatic baseline-correction method for multidimensional NMR spectra with strong solvent signals. *J. Magn. Reson. Ser. A,* **117**, 330–333.

Bartels, C., Xia, T., Billeter, M., Güntert, P. & Wüntert, K. (1995b). The program XEASY for computer-supported NMR spectral analysis of biological macromolecules. *J. Biomol. NMR,* **6**, 1–10.

Bax, A. & Pochapsky, S. S. (1992). Optimized recording of heteronuclear multidimensional NMR spectra using pulsed field gradients. *J. Magn. Reson.* **99**, 638–643.

Bax, A., Clore, G. M. & Gronenborn, A. M. (1990). ^{1}H-^{1}H correlation via isotropic mixing of ^{13}C magnetization, a new three-dimensional approach for assigning ^{1}H and ^{13}C spectra of ^{13}C enriched proteins. *J. Magn. Reson.* **88**, 425–431.

Bax, A., Delaglio, F., Grzesiek, S. & Vuister, G. W. (1994). Resonance assignment of methionine methyl groups and χ^3 angular information from long-range proton-carbon and carbon-carbon J correlation in a calmodulin-peptide complex. *J. Biomol. NMR,* **4**, 787–797.

Billeter, M., Schaumann, T., Braun, W. & Wüthrich, K. (1990). Restrained energy refinement with two different algorithms and force fields of the structure of the α-amylase inhibitor tendamistat determined by NMR in solution. *Biopolymers,* **29**, 695–706.

Bodenhausen, G. & Ruben, D. J. (1980). Natural abundance nitrogen-15 NMR by enhanced heteronuclear spectroscopy. *Chem. Phys. Letters,* **69**, 185–189.

Borel, J. F. (1986). Editor of *Ciclosporin,* Karger, Basel.

Borel, J. F. (1989). Pharmacology of cyclosporin (Sandimmune) IV. Pharmacological properties *in vivo*. *Pharmacol. Rev.* **41**, 259–371.

Braun, W., Kallen, J., Mikol, V., Walkinshaw, M. D. & Wüthrich, K. (1995). Three-dimensional structure and actions of immunosuppressants and their immunophilins. *FASEB J.* **9**, 63–72.

Braunschweiler, L. & Ernst, R. R. (1983). Coherence transfer by isotropic mixing: application to proton correlation spectroscopy. *J. Magn. Reson.* **53**, 521–528.

Chary, K. V. R., Otting, G. & Wüthrich, K. (1991). Measurement of small heteronuclear ^{1}H-^{15}N coupling constants in ^{15}N-labeled proteins by 3D H_NNH_{AB}-COSY. *J. Magn. Reson.* **93**, 218–224.

Cheng, J. W., Lepre, C. A., Chambers, S. P., Fulghum, J. R., Thomson, J. A. & Moore, J. M. (1993). ^{15}N NMR relaxation studies of the FK506 binding protein: backbone dynamics of the uncomplexed receptor. *Biochemistry,* **32**, 9000–9010.

Cheng, J. W., Lepre, C. A. & Moore, J. M. (1994). ^{15}N NMR relaxation studies of the FK506 binding protein: dynamic effects of ligand binding and implications for calcineurin recognition. *Biochemistry,* **33**, 4093–4100.

Clubb, R. T., Ferguson, S. B., Walsh, C. T. & Wagner, G. (1994). Three-dimensional solution structure of *Escherichia coli* periplasmic cyclophilin. *Biochemistry,* **33**, 2761–2772.

Edison, A. S., Westler, W. M. & Markley, J. L. (1991). Elucidation of amino acid spin systems in proteins and determination of heteronucler coupling constants by carbon-proton-proton three-dimensional NMR. *J. Magn. Reson.* **92**, 434–438.

Fesik, S. W. & Zuiderweg, E. R. P. (1988). Heteronuclear three-dimensional NMR spectroscopy. A strategy for the simplification of homonuclear two-dimensional NMR spectra. *J. Magn. Reson.* **78**, 588–593.

Fesik, S. W., Gampe, R. T., Eaton, H. L., Gemmecker, G., Olejnizak, E. T., Neri, P., Egan, D. A., Edalji, R., Simmer, R., Helfrich, R., Hochlowski, J. & Jackson, M. (1991). NMR studies of [U-^{13}C]cyclosporin A bound to cyclophilin: bound conformation and portions of cyclosporin involved in binding. *Biochemistry,* **30**, 6574–6583.

Fischer, G., Wittmann-Liebold, B., Lang, K., Kiefhaber, T. & Schmid, F. X. (1989). Cyclophilin and peptidyl-prolyl *cis-trans* isomerase are probably identical proteins. *Nature,* **337**, 476–478.

Fogh, R. H., Schipper, D., Boelens, R. & Kaptein, R. (1995). Complete ^{1}H, ^{13}C and ^{15}N NMR assignments and secondary structure of the 269-residue serine protease PB92 from *Bacillus alcalophilus*. *J. Biomol. NMR,* **5**, 259–270.

Franke, E. K., Yuan, H. E. & Luban, J. (1994). Specific incorporation of cyclophilin A into HIV-1 virions. *Nature,* **372**, 359–362.

Gamble, T. R., Vajdos, F. F., Yoo, S., Worthylake, D. K., Houseweart, M., Sundquist, W. I. & Hill, C. P. (1996). Crystal structure of human cyclophilin A bound to the amino-terminal domain of HIV-1capsiol. *Cell,* **87**, 1285–1294.

Griesinger, C., Otting, C., Wüthrich, K. & Ernst, R. R. (1988). Clean-TOCSY for ^{1}H spin system identification in macromolecules. *J. Am. Chem. Soc.* **110**, 7870–7872.

Griffith, J. P., Kim, J. L., Kim, E. E., Sintchak, M. D., Thomson, J. A., Fitzgibbon, M. J., Fleming, M. A., Caron, P. R., Hsiao, K. & Navia, M. A. (1995). X-ray structure of calcineurin inhibited by the immunophilin-immunosuppressant FKBP12-FK506 complex. *Cell,* **82**, 507–522.

Grzesiek, S. & Bax, A. (1992). Correlating backbone amide and side chain resonances in larger proteins by multiple relayed triple resonance NMR. *J. Am. Chem. Soc.* **114**, 6291–6293.

Grzesiek, S. & Bax, A. (1993). Amino acid type determination in the sequential assignment procedure of uniformly $^{13}C/^{15}N$-enriched proteins. *J. Biomol. NMR,* **3**, 185–204.

Güntert, P. & Wüthrich, K. (1991). Improved efficiency of protein structure calculations from NMR data using the program DIANA with redundant dihedral angle constraints. *J. Biomol. NMR,* **1**, 447–456.

Güntert, P., Braun, W., Billeter, M. & Wüthrich, K. (1989). Automated stereospecific ^{1}H NMR assignments and their impact on the precision of protein structure determinations in solution. *J. Am. Chem. Soc.* **111**, 3997–4004.

Güntert, P., Braun, W. & Wüthrich, K. (1991). Efficient computation of three-dimensional protein structures in solution from nuclear magnetic resonance data using the program DIANA and the supporting programs CALIBA, HABAS and GLOMSA. *J. Mol. Biol.* **217**, 517–530.

Güntert, P., Dötsch, V., Wider, G. & Wüthrich, K. (1992). Processing of multi-dimensional NMR data with the new software PROSA. *J. Biomol. NMR,* **2**, 619–629.

Güntert, P., Berndt, K. D. & Wüthrich, K. (1993). The program ASNO for computer-supported collection of NOE upper distance constraints as input for protein structure determination. *J. Biomol. NMR,* **3**, 601–606.

Handschumacher, R. E., Harding, M. W., Rice, J., Drugge, R. J. & Speicher, D. W. (1984). Cyclophilin: a specific cytosolic binding protein for cyclosporin A. *Science,* **226**, 544–547.

Holm, L. & Sander, C. (1993). Protein structure comparison by alignment of distance matrices. *J. Mol. Biol.* **233**, 123–138.

Ikura, M., Kay, L. E., Tschudin, R. & Bax, A. (1990). Three-dimensional NOESY-HMQC spectroscopy of a ^{13}C-labeled protein. *J. Magn. Reson.* **86**, 204–209.

Ikura, M., Kay, L. E. & Bax, A. (1991). Improved three-dimensional ^{1}H-^{13}C-^{1}H correlation spectroscopy of a ^{13}C-labeled protein using constant-time evolution. *J. Biomol. NMR,* **1**, 299–304.

Kallen, J. & Walkinshaw, M. D. (1992). The X-ray structure of a tetrapeptide bound to the active site of human cyclophilin A. *FEBS Letters,* **300**, 286–290.

Kallen, J., Spitzfaden, C., Zurini, M. G. M., Wider, G., Widmer, H., Wüthrich, K. & Walkinshaw, M. D. (1991). Structure of human cyclophilin and its binding site for cyclosporin A determined by X-ray crystallography and NMR spectroscopy. *Nature,* **353**, 276–279.

Kay, L. E., Ikura, M. & Bax, A. (1990). Proton-proton correlation via carbon–carbon couplings: a three-dimensional NMR approach for the assignment of aliphatic resonances in proteins labeled with carbon-13. *J. Am. Chem. Soc.* **112**, 888–889.

Ke, H. (1992). Similarities and differences between human cyclophilin A and other β-barrel structures. *J. Mol. Biol.* **228**, 539–550.

Ke, H., Zydowsky, L. D., Liu, J. & Walsh, C. T. (1991). Crystal structure of recombinant human T-cell

cyclophilin A. at 2.5 Å resolution. *Proc. Natl Acad. Sci. USA,* **88**, 9483–9487.

Ke, H., Mayrose, D. & Cao, W. (1993a). Crystal structure of cyclophilin A complexed with substrate Ala-Pro suggests a solvent-assisted mechanism of *cis-trans* isomerization. *Proc. Natl Acad. Sci. USA,* **90**, 3324–3328.

Ke, H., Zhao, Y., Luo, F., Weissman, I. & Friedman, J. (1993b). Crystal structure of murine cyclophilin C complexed with immunosuppressive drug cyclosporin A. *Proc. Natl Acad. Sci. USA,* **90**, 11850–11854.

Ke, H., Mayrose, D., Belshaw, P. J., Alberg, D. G., Schreiber, S. L., Chang, Z. Y., Etzkorn, F. A., Ho, S. & Walsh, C. T. (1994). Crystal structures of cyclophilin A complexed with cyclosporin A and N-methyl-4-[(E)-2-butenyl]-4,4-dimethylthreonine cyclosporin A. *Structure,* **2**, 33–44.

Kissinger, C. R., Parge, H. E., Knighton, D. R., Lewis, C. T., Pelletier, L. A., Tempzyk, A., Kalish, V. J., Tucker, K. D., Showalter, R. E., Moomaw, E. W., Gastinel, L. N., Habuka, N., Chen, X., Maldonado, F., Baker, J. E., Bacquet, R. & Villafranca, J. E. (1995). Crystal structures of human calcineurin and the human FKBP12-FK506-calcineurin complex. *Nature,* **378**, 641–644.

Konno, M., Ito, M., Hayano, T. & Takahashi, N. (1996). The substrate-binding site in *Escherichia coli* cyclophilin A preferably recognizes a *cis*-proline isomer or a highly distorted form of the *trans* isomer. *J. Mol. Biol.* **256**, 897–908.

Koradi, R., Billeter, M. & Wüthrich, K. (1996). MOLMOL: a program for display and analysis of macromolecular structures. *J. Mol. Graph.* **14**, 52–55.

Levitt, M. (1983). Protein folding by restrained energy minimization and molecular dynamics. *J. Mol. Biol.* **170**, 723–764.

Lima, C. D., Wang, J. C. & Mondragón, A. (1994). Three-dimensional structure of the 67K N-terminal fragment of *E. coli* DNA topoisomerase I. *Nature.* **367**, 138–146.

Loosli, H. R., Kessler, H., Oschkinat, H., Weber, H. P., Petcher, T. J. & Widmer, A. (1985). The conformation of cyclosporin A in the crystal and in solution. *Helv. Chim. Acta,* **68**, 682–704.

Luban, J., Bossolt, K. L., Franke, E. K., Kalpana, G. V. & Goff, S. P. (1993). Human immunodeficiency virus type 1 Gag protein binds to cyclophilins A and B. *Cell,* **73**, 1067–1078.

Luginbühl, P., Güntert, P., Billeter, M. & Wüthrich, K. (1996). The new program OPAL for molecular dynamics simulations and energy refinements of biological macromolecules. *J. Biomol. NMR,* **8**, 136–146.

Madsen, J. C. & Sørensen, O. W. (1992). Multidimensional NMR experiments with improved resolution. *J. Magn. Reson.* **100**, 431–436.

Marion, D., Ikura, M., Tschudin, R. & Bax, A. (1989). Rapid recording of 2D NMR spectra without phase cycling: application to the study of hydrogen exchange in proteins. *J. Magn. Reson.* **85**, 393–399.

Messerle, B. A., Wider, G., Otting, G., Weber, C. & Wüthrich, K. (1989). Solvent suppression using a spin lock in 2D and 3D NMR spectroscopy with H_2O solutions. *J. Magn. Reson.* **85**, 608–613.

Mikol, V., Kallen, J., Pflügl, G. & Walkinshaw, M. D. (1993). X-ray structure of a monomeric cyclophilin A-cyclosporin A crystal complex at 2.1 Å resolution. *J. Mol. Biol.* **234**, 1119–1130.

Mikol, V., Kallen, J. & Walkinshaw, M. D. (1994a). The X-ray structure of $(MeBm_{2t})^1$-cyclosporin complexed with cyclophilin A provides an explanation for its anomalously high immunosuppressive activity. *Protein Eng.* **7**, 597–603.

Mikol, V., Kallen, J. & Walkinshaw, M. D. (1994b). X-ray structure of a cyclophilin B/cyclosporin complex: comparison with cyclophilin A and delineation of its calcineurin-binding domain. *Proc. Natl Acad. Sci. USA,* **91**, 5183–5186.

Mikol, V., Papageorgiou, C. & Borer, X. (1995). The role of water molecules in the structure-based design of (5-hydroxynorvaline)-2-cyclosporin: synthesis, biological activity, and crystallographic analysis with cyclophilin A. *J. Med. Chem.* **38**, 3361–3367.

Neri, D., Szyperski, T., Otting, G., Senn, H. & Wüthrich, K. (1989). Stereospecific nuclear magnetic resonance assignments of the methyl groups of valine and leucine in the DNA-binding domain of the 434 repressor by biosynthetically-directed fractional ^{13}C labeling. *Biochemistry,* **28**, 7510–7516.

Otting, G. & Wüthrich, K. (1990). Heteronuclear filters in two-dimensional [^1H, ^1H]-NMR spectroscopy: combined use with isotope labelling for studies of macromolecular conformation and intermolecular interactions. *Quart. Rev. Biophys.* **23**, 39–96.

Papageorgiou, C., Florineth, A. & Mikol, V. (1994). Improved binding affinity for cyclophilin A by a cyclosporin derivative singly modified at its effector domain. *J. Med. Chem.* **37**, 3674–3676.

Peng, J. W. & Wagner, G. (1994). Investigation of protein motions *via* relaxation measurements. *Methods Enzymol.* **239**, 563–596.

Perkins, S. J. & Wüthrich, K. (1979). Ring current effects in the conformation-dependent NMR chemical shifts of aliphatic proteins in the basic pancreatic trypsin inhibitor. *Biochim. Biophys. Acta,* **576**, 409–423.

Pflügl, G., Kallen, J., Schirmer, T., Jansonius, J. N., Zurini, M. G. M. & Walkinshaw, M. D. (1993). X-ray structure of a decameric cyclophilin-cyclosporin crystal complex. *Nature,* **361**, 91–94.

Pflügl, G., Kallen, J., Jansonius, J. N. & Walkinshaw, M. D. (1994). The molecular replacement solution and X-ray refinement to 2.8 Å of a decameric complex of human cyclophilin A with the immunosuppressive drug cyclosporin A. *J. Mol. Biol.* **244**, 385–409.

Sambrook, J., Fritsch, E. F. & Maniatis, T. (1989). *Molecular Cloning: A Laboratory Manual,* Cold Spring Harbor Laboratory Press, Plainview, New York.

Schreiber, S. L. (1991). Chemistry and biology of the immunophilins and their immunosuppressant ligands. *Science.* **251**, 283–287.

Senn, H., Werner, B., Messerle, B. A., Weber, C., Traber, R. & Wüthrich, K. (1989). Stereospecific assignments of the methyl ^1N NMR lines of valine and leucine in polypeptides by nonrandom ^{13}C labelling. *FEBS Letters,* **249**, 113–118.

Spitzfaden, C., Weber, H. P., Braun, W., Kallen, J., Wider, G., Widmer, H., Walkinshaw, M. D. & Wüthrich, K. (1992). Cyclosporin A-cyclophilin complex formation. A model based on X-ray and NMR data. *FEBS Letters,* **300**, 291–300.

Spitzfaden, C., Braun, W., Wider, G., Widmer, H. & Wüthrich, K. (1994). Determination of the NMR solution structure of the cyclophilin-cyclosporin A complex. *J. Biomol. NMR,* **4**, 463–482.

Szyperski, T., Güntert, P., Otting, G. & Wüthrich, K. (1992). Determination of scalar coupling constants by inverse Fourier transformation of in-phase multiples. *J. Magn. Reson.* **99**, 552–560.

Szyperski, T., Luginbühl, P., Otting, G., Güntert, P. & Wüthrich, K. (1993). Protein dynamics studied by rotating frame ^{15}N spin relaxation times. *J. Biomol. NMR*, **3**, 151–164.

Thali, M., Bukovsky, A., Kondo, E., Rosenwirth, B., Walsh, C. T., Sodroski, J. & Göttlinger, H. G. (1994). Functional association of cyclopholin A with HIV-1 virions. *Nature*, **372**, 363–365.

Thériault, Y., Logan, T. M., Meadows, R., Yu, L., Olejniczak, E. T., Holzman, T. F., Simmer, R. L. & Fesik, S. W. (1993). Solution structure of the cyclosporin A/cyclophilin complex by NMR. *Nature*, **361**, 88–91.

Vuister, G. W. & Bax, A. (1992). Resolution enhancement and spectral editing of uniformly ^{13}C-enriched proteins by homonuclear broadband ^{13}C decoupling. *J. Magn. Reson.* **98**, 428–435.

Weber, C., Wider, G., von Freyberg, B., Traber, R., Braun, W., Widmer, H. & Wüthrich, K. (1991). The NMR structure of cyclosporin A bound to cyclophilin in aqueous solution. *Biochemistry*, **30**, 6563–6574.

Weiner, S. J., Kollman, P. A., Nguyen, D. T. & Case, D. A. (1986). An all atom force field for simulations of proteins and nucleic acids. *J. Comput. Chem.* **7**, 230–252.

Wider, G. & Wüthrich, K. (1993). A simple experimental scheme using pulsed field gradients for coherence-pathway rejection and solvent suppression in phase-sensitive heteronuclear correlation spectra. *J. Magn. Reson. Ser. B*, **102**, 239–241.

Wüthrich, K. (1986). *NMR of Proteins and Nucleic Acids*, Wiley, New York.

Wüthrich, K., Billeter, M. & Braun, W. (1983). Pseudo-structures for the 20 common amino acids for use in studies of protein conformations by measurements of intramolecular proton-proton distance constraints with nuclear magnetic resonance. *J. Mol. Biol.* **169**, 949–961.

Wüthrich, K., Billeter, M. & Braun, W. (1984). Polypeptide secondary structure determination by nuclear magnetic resonance observation of short proton-proton distances. *J. Mol. Biol.* **180**, 715–740.

Wüthrich, K., Spitzfaden, C., Memmert, K., Widmer, H. & Wider, G. (1991a). Protein secondary structure determination by NMR: application with recombinant human cyclophilin. *FEBS Letters*, **285**, 237–247.

Wüthrich, K., von Freyberg, B., Weber, C., Wider, G., Traber, R., Widmer, H. & Braun, W. (1991b). Receptor-induced conformation change of the immunosuppressant cyclosporin A. *Science*, **254**, 953–954.

Yamazaki, T., Kay, J. D. & Kay, L. E. (1993). Two-dimensional NMR experiments for correlating $^{13}C^{\beta}$ and $^{1}H^{\delta/\varepsilon}$ chemical shifts of aromatic residues in ^{13}C labeled proteins *via* scalar couplings. *J. Am. Chem. Soc.* **115**, 11054–11055.

Zerbe, O., Szyperski, T., Ottiger, M. & Wüthrich, K. (1996). Three-dimensional ^{1}H-TOCSY-relayed ct-[^{13}C, ^{1}H]-HMQC for aromatic spin system identification in uniformly ^{13}C labeled proteins. *J. Biomol. NMR*, **7**, 99–106.

Zhao, Y. & Ke, H. (1996a). Crystal structure implies that cyclophilin predominantly catalyzes the *trans* to *cis* isomerization. *Biochemistry*, **35**, 7356–7361.

Zhao, Y. & Ke, H. (1996b). Mechanistic implication of crystal structures of the cyclophilin-dipeptide complexes. *Biochemistry*, **35**, 7362–7368.

Zhao, Y., Chen, Y., Schutkowski, M., Fischer, G. & Ke, H. (1997). Cyclophilin A complexed with a fragment of HIV-1 gag protein: insights into HIV-1 infectious activity. *Structure*, **5**, 139–146.

Edited by P. E. Wright

(Received 7 March 1997; received in revised form 2 June 1997; accepted 10 June 1997)

http://www.hbuk.co.uk/jmb

Supplementary material comprising three Tables is available from JMB Online